ChemPhotoChem

Research Article
doi.org/10.1002/cptc.202400023

Chemistry Europe
European Chemical Societies Publishing

www.chemphotochem.org

Comparison of Vinyldimethylaniline and Indolizine Donor Groups on Si-Substituted Xanthene Core Shortwave Infrared Fluorophores

Ravinder Kaur,[a] Nicholas A. Kruse,[a] Cameron Smith,[a] Nathan I. Hammer,[a] and Jared H. Delcamp*[a, b]

Small organic molecules absorbing and emitting in the shortwave infrared (SWIR, 1000–2000 nm) region are desirable for biological imaging applications due to low auto-fluorescence, reduce photon scattering, and good tissue penetration depth of photons which allows for *in vivo* imaging with high resolution and sensitivity. Si-substituted xanthene-based fluorophores with indolizine donors have demonstrated some of the longest wavelengths of absorption and emission from organic dyes. This work seeks to compare an indolizine heterocyclic nitrogen with dimethyl aniline nitrogen donors on otherwise identical Si-substituted xanthene fluorophores *via* optical spectroscopy, computational chemistry and electrochemistry. Three donors are compared including an indolizine donor, a ubiquitous dimethyl aniline donor, and a vinyl dimethyl aniline group that keeps the number of π-bonds consistent with indolizine. Significantly higher quantum yields and molar absorptivity are observed in these studies for a dimethylamine-based donor relative to a simple indolizine donor absorbing and emitting at similar wavelengths (~1312 nm emission). Substantially longer wavelengths are obtainable by appending aniline-based groups to the indolizine donor (~1700 nm) indicating longer wavelengths can be accessed with indolizine donors while stronger emitters can be accessed with anilines in place of indolizine.

Introduction

Fluorescence imaging is a powerful techniques for non-invasive visualization of living systems with high temporal and spatial resolution.[1] Small organic molecules are extensively studied as potential fluorescent probes due to advantages such as tailorable designs, biocompatibility, fast excretion rate, and lack of long-term toxic effects.[2] Fluorescent probes which can absorb and emit in the near infrared-II region (NIR-II, 1000–1700 nm) or shortwave infrared region (SWIR) (1000–2000 nm) offer deeper tissue imaging than higher energy spectral regions, reduced imaging noise due to low autofluorescence, and higher contrast images due to low tissue photon scattering coefficients at longer wavelengths.[3] Xanthene dyes such as fluorescein, rosamines, and rhodamines have many favorable characteristics for bioimaging, including high molecular brightness (MB), good fluorescence quantum yields (Φ), and high molar extinction coefficient (ε) values. These characteristics have led to the widespread use of xanthene dyes as fluorescent cores for various sensor probes and in bioimaging applications.[4] However, xanthene dyes absorbing in SWIR region (> 1000 nm) have low MB values primarily due to low quantum yields at longer wavelengths.[3e,5] MB is the product of the Φ and the ε of a material at the corresponding excitation wavelength. A high MB value of a fluorophore can improve imaging speed, the quality of the imaging signal, and provide high resolution images with minimized dye dosage.[3c,6] Thus, fluorophores with a high MB and Φ that absorbs and emit in the SWIR region could improve the accuracy, quality, and imaging response time of non-invasive *in vivo* fluorescence imaging. While a strong signal (high MB) is desirable, we note that even low signals in longer wavelength regions can give clear *in vivo* images due to very low background noise (low autofluorescence and reduced scattering) found in the SWIR region and beyond which allows dyes of low MB to retain practical value.[7]

Derivatization group selection on a fluorophore such as xanthene can have a dramatic impact on emission wavelength, MB, and Φ. Synthetic strategies to obtain molecules with altered photophysical properties includes extension of the π-conjugation of the xanthene chromophore, modification of the donor group appended to the xanthene core, and replacement of the central oxygen atom with other elements. Fu and co-workers reported that Si-substituted xanthene-core based fluorophores exhibit far red to near infrared absorption and emission.[8] Herein, the photophysical properties imparted by donor groups appended to a consistent Si-substituted xanthene-based fluorophore core (SiRos) are compared with varied structure and conjugation lengths. *N*,*N*-dimethylaniline (DMA) is a commonly used donor with NIR and SWIR emitting materials appended to Si-substituted xanthene to give **SiRosDMA** in this study (Figure 1).

Recently, we have found nitrogen heterocycle indolizine-based donors to allow for dramatic shifts into the SWIR region

[a] *R. Kaur, N. A. Kruse, C. Smith, N. I. Hammer, J. H. Delcamp*
Department of Chemistry, University of Mississippi, University, MS 38677
E-mail: delcamp@olemiss.edu

[b] *J. H. Delcamp*
Present Address: Air Force Research Laboratory, Materials and Manufacturing Directorate (RXNC), Wright-Patterson AFB, OH-45433, USA

Supporting information for this article is available on the WWW under https://doi.org/10.1002/cptc.202400023

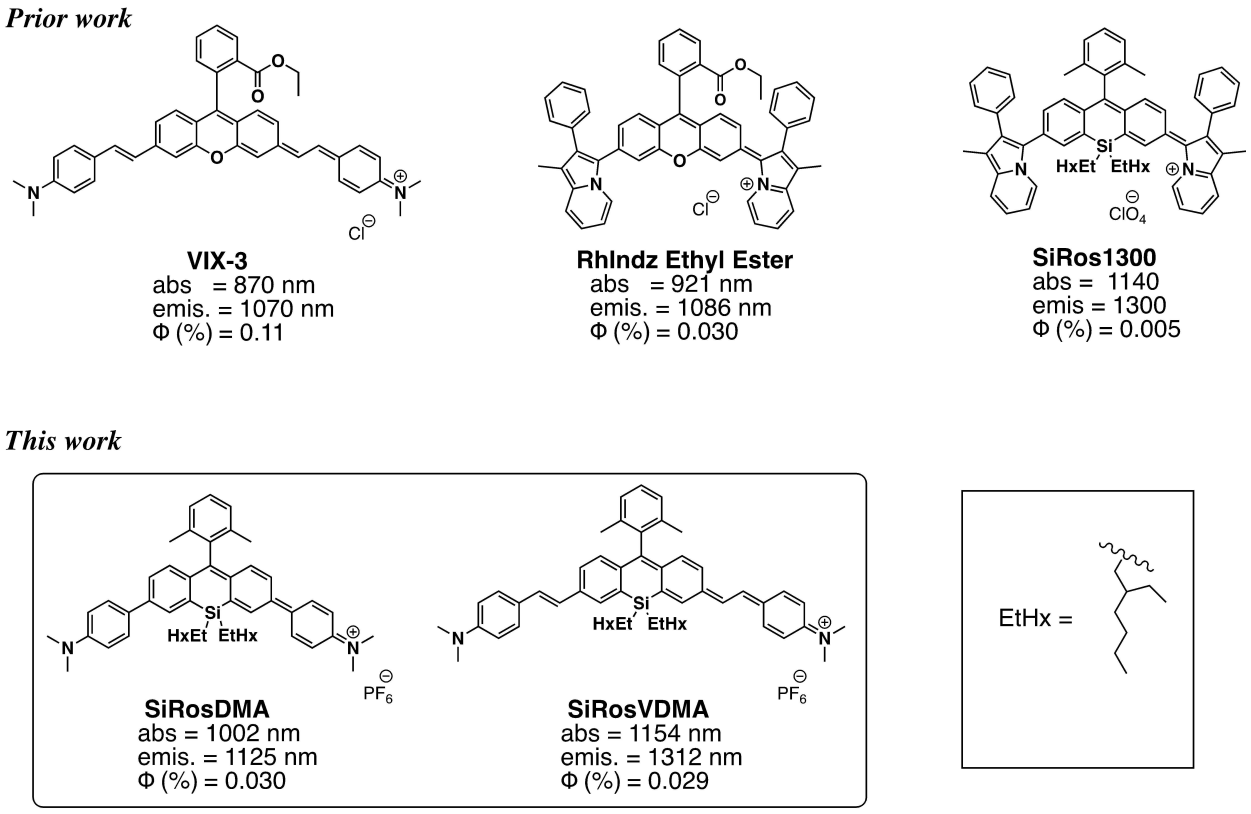

Figure 1. Comparison of absorption (abs), emission (emis) and fluorescence quantum yield (Φ) of dyes from prior work **VIX-3**,[3e] **RhIndz Ethyl Ester**,[9c] and **SiRos1300**[7] with dyes from this work **SiRosVDMA** and **SiRosDMA**.

for cyanine, BODIPY, rhodamine (**RhIndz** in Figure 1), xanthenes, and Si-substituted xanthenes (**SiRos1300** in Figure 1).[5,7,9] While indolizine has allowed for shifting of chromophores to longer wavelengths than DMA, it is unclear if this is due to the extended conjugation of indolizine (4-π bonds and an electron pair on nitrogen with indolizine versus 3-π bonds and an electron pair with DMA) or due to an increased donation strength because of better overlap of the π-system with the planarized nitrogen atom donor with indolizine which does not have out of π-system plane rotation possibilities such as with DMA. To separate these effects, vinyl *N*, *N*-dimethylaniline (VDMA) is appended as a donor on SiRos to give **SiRosVDMA** where VDMA has the same number of π-bonds and nitrogen donor electrons as indolizine (Figure 1). Recently, VDMA has been used on xanthene to give dye **VIX-3** which is a SWIR emitter (Figure 1). A similar absorption and emission profile between VDMA and indolizine-based dyes would indicate conjugation is the primary effect, while a significant shift in peak absorption and emission properties would suggest a unique donation ability of indolizine relative to VDMA. In addition to the shifting of absorption and emission wavelengths, these three derivatives are evaluated for the effect of the donor groups on MB and Φ. The effect of these donors on Si-substituted xanthene fluorophore properties was further investigated computationally and electrochemically.

Results and Discussion

The target dyes (**SiRosDMA** and **SiRosVDMA**) along with **SiRos1300** were first analyzed computationally. Geometry optimizations via density functional theory (DFT) and time-dependent density functional theory (TD-DFT) were conducted for the dyes at the B3LYP/6-311g (d,p)[10] level of theory using dichloromethane as an implicit solvent via a polarizable continuum model with Gaussian16 software (Figure 2 and Table 1).[11] Frontier molecular orbitals distribution shows delocalization of the highest occupied molecule orbital (HOMO) across the core and donor groups of the dyes in all cases. Similarly, the lowest unoccupied molecular orbital (LUMO) is delocalized across the π-conjugated dye system. Accordingly,

Table 1. Computational data for **SiRosDMA**, **SiRosVDMA**, and **SiRos1300** computed at the B3LYP/6-311G(d,p) level of theory using dichloromethane as a solvent.

Dye	HOMO (eV)	LUMO (eV)	Vert. Trans. (eV)	Oscillator Strength	Dihedral Angle (°)
SiRosDMA	−5.62	−4.02	1.52	1.85	20.6
SiRosVDMA	−5.39	−3.97	1.36	2.56	0.9
SiRos1300	−5.50	−4.01	1.39	1.48	35.3

The vertical transitions (vert. trans.) reported are all S_0 to S_1 with > 98% of the contribution to this transition being the HOMO to LUMO transition.

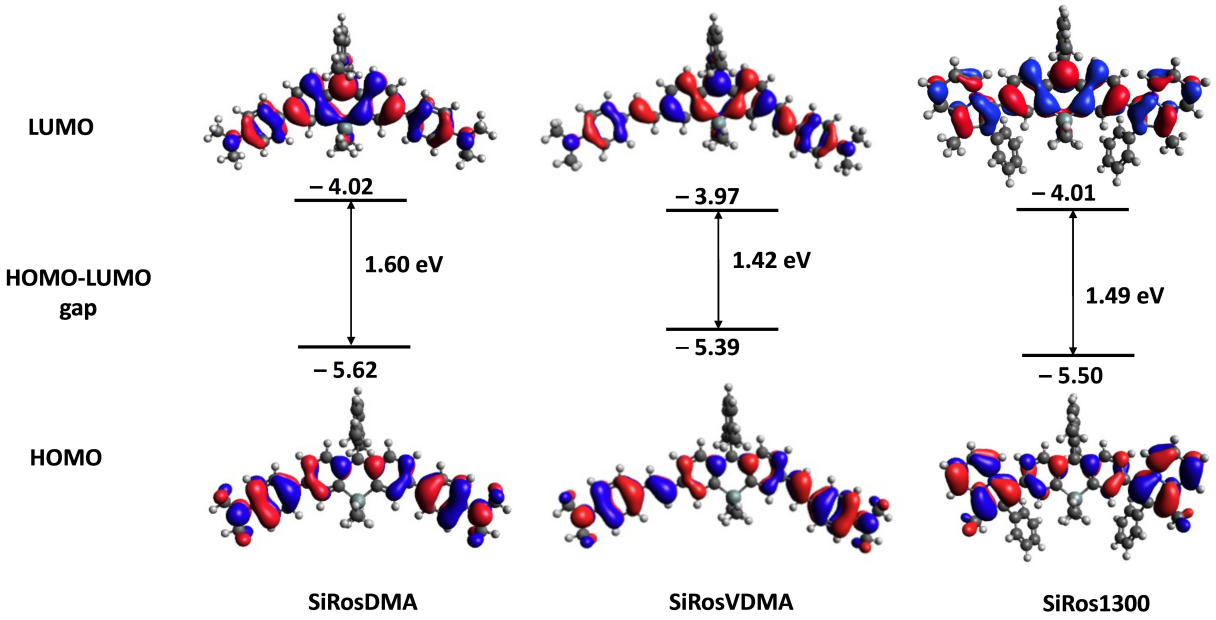

Figure 2. HOMO (bottom) and LUMO (top) of the SiRos dyes computed at the B3LYP/6-311G (d,p) level of theory using dichloromethane as an implicit solvent.

there is good overlap of the HOMO and LUMO in all cases which suggests strong oscillator strengths should be observed for the HOMO to LUMO transition as is common for cyanine-type dye $\pi \rightarrow \pi^*$ transitions. The HOMO-LUMO energy gap is largest for **SiRosDMA** at 1.60 eV, followed by **SiRos1300** (1.49 eV) and then **SiRosVDMA** (1.42 eV). This trend suggests a significantly lower energy absorption is anticipated for **SiRos1300** and **SiRosVDMA** than **SiRosDMA** which indicates the donors with more π-conjugated bonds are likely to absorb at longer wavelengths. Additionally, the dihedral angles observed between the donor and core bonds decreases in the following order: **SiRos1300** (35.3°) > **SiRosDMA** (20.6°) > **SiRosVDMA** (0.9°). This trend illustrates the steric congestion at the donor-core bond and can significantly influence the dye molar absorptivity with reduced dihedral angles typically having high molar absorptivities. Since the core is held constant, the donor sizes are in the following order at the point where the core is bonded: indolizine > DMA > VDMA.

The TD-DFT predicted vertical transition energy trend for the S_0 to S_1 transition shows **SiRosDMA** > **SiRos1300**≅**SiRosVDMA** ranging from 1.52 eV to 1.36 eV indicating **SiRosVDMA** is predicted to have the lowest energy absorption (Table 1). Notably, all S_0 to S_1 transitions were observed to be > 98% HOMO to LUMO in composition. This indicates good orbital overlap is present for the lowest energy transition and cyanine-like strong oscillator strengths are anticipated. The oscillator strength for the lowest energy vertical transitions follows the same trend as observed by the dihedral angle about the donor and core with **SiRosVDMA** at 2.56, **SiRosDMA** at 1.85, and **SiRos1300** at 1.48. This trend again suggests the molar absorptivity of these dyes will be strongest when the VDMA donor is used and weakest when indolizine is used.

The target dyes **SiRosDMA** and **SiRosVDMA** dyes were synthesized as described in Scheme 1. The synthesis of the **SiRosDMA** begins with a Suzuki coupling of Si-substituted xanthene core **1** and *N*, *N*-dimethyl-4-(4,4,5,5 tetramethyl-1,3,2-dioxaborolan-2-yl)aniline (**2**) to give ketone **3** in 71% yield. The synthesis of **SiRosVDMA** begins with the Heck coupling of Si-substituted xanthene core **1** and *N*, *N*-dimethyl-4-vinylaniline (**4**) to give ketone **5** in 89% yield. Ketones **3** and **5** react with the Grignard reagent 2,6-dimethylphenylmagnesium bromide followed by work up with water to convert the alkoxide species to the corresponding alcohols as intermediates that were directly used in the next steps without isolation. The final dyes were synthesized by exposure to $POCl_3$ followed by addition of excess KPF_6 to give the final products (**SiRosDMA** and **SiRosVDMA**) with 63% and 49% yield, respectively.

The visible-near infrared-shortwave infrared (Vis-NIR-SWIR) absorption and fluorescence spectra of the dyes were taken in dichloromethane (CH_2Cl_2). The absorption maximum (λ_{abs}) of **SiRosDMA** is observed at 1002 nm. Inserting a carbon-carbon double bond between the DMA donor and the Si-substituted xanthene core shifted λ_{abs} to 1154 nm with **SiRosVDMA** (Figure 3, Table 2). The shift to longer wavelength in λ_{abs} upon addition of the two double bonds is observed to be 152 nm (0.16 eV). **SiRos1300** with indolizine donors has a λ_{abs} of 1140 nm which is similar to **SiRosVDMA**.[7] The similar λ_{abs} value observed when VDMA and indolizine are used as donors (~0.01 eV difference) suggests a similar donation strength of the nitrogen electrons in both systems since the number of π-bonds at the donor groups is constant at 4 π-bonds. The molar absorptivity coefficient (ε) of **SiRosDMA** is 128,500 $M^{-1}cm^{-1}$ with **SiRosVDMA** at 141,000 $M^{-1}cm^{-1}$. The higher ε value with the VDMA donor is expected due to the reduced steric interactions between the alkene of the donor and Si-substituted xanthene core relative to the steric interactions of a phenyl ring and the Si-substituted xanthene core. Computationally, the dihedral angle observed at the donor-core bond is significantly

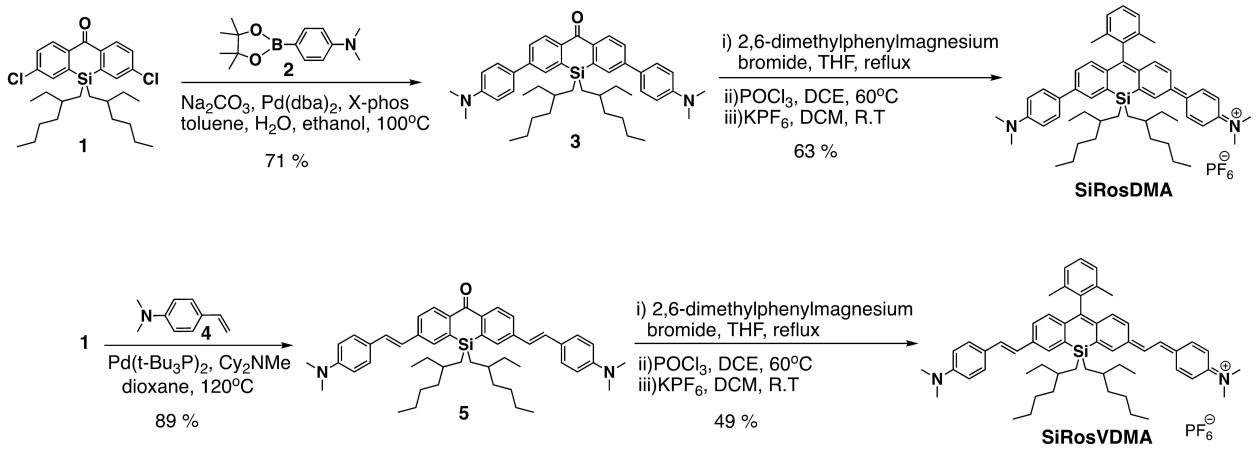

Scheme 1. Synthetic route to **SiRosDMA** and **SiRosVDMA**.

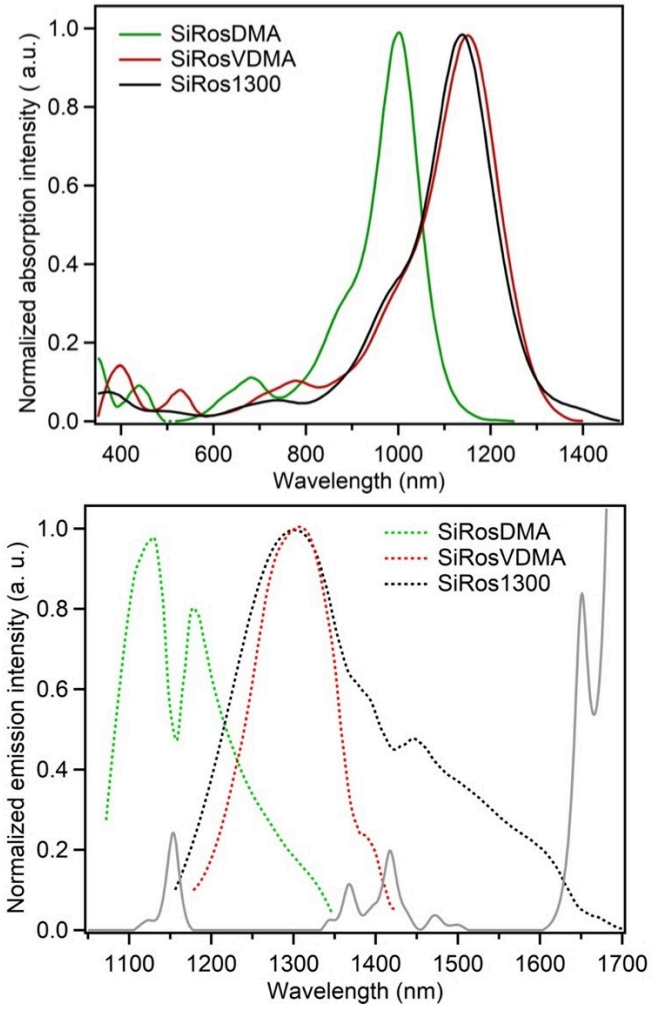

Figure 3. Absorption (top) and emission (bottom) of **SiRosDMA**, **SiRosVDMA** and **SiRos1300** in CH_2Cl_2. The solid grey line on the bottom graph along with the dotted lines representing emission is the absorption spectrum of DCM. The drops in the emission spectrum at approximately 1150 nm, 1380 nm, 1425 nm, and 1650 nm correspond to solvent absorption. The sharp dip around 1150 nm in the **SiRosDMA** emission curve is due to DCM solvent absorption which arises from overtones of the stretching vibrations of C–H bonds of DCM.[12]

lower for **SiRosVDMA** than **SiRosDMA** (0.9° versus 20.6° Table 1). We reasoned that the indolizine donor would have further increased sterics at the donor-Si-substituted xanthene core (dihedral angle of 35.3°), and the lower ε value observed for **SiRos1300** suggests this may be correct at 115,000 $M^{-1}cm^{-1}$. The ε trend (**SiRosVDMA** > **SiRosDMA** > **SiRos1300**) is the same as that observed for the oscillator strengths computationally (Table 1). Computationally, the dihedral angle at the donor-Si-substituted xanthene core also correlates to the ε trend observed suggesting that steric interactions at this site induces changes in the molar absorptivity.

The fluorescence spectra of **SiRosDMA** and **SiRosVDMA** have emission maxima (λ_{em}) at 1125 nm and 1312 nm, respectively (Table 2). **SiRos1300** is observed to emit at a similar wavelength to **SiRosVDMA** (1300 nm versus 1312 nm, respectively), which suggest similar donor strengths when VDMA and indolizine are compared. The Stokes shift (the difference between λ_{abs} and λ_{em}) is similar for all three dyes at 0.13–0.14 eV which indicates the dyes all have a similar reorganization energy upon changing geometries between the ground and excited states. The Φ values for each of the Si-substituted xanthene core dyes were measured using **IR-1061** as a standard and taking the Φ value of this dye to be 0.32%.[13] The Φ value of **SiRosDMA** was found be similar to **SiRosVDMA** at 0.030% and 0.029%, respectively. These Φ values are appreciably higher than **SiRos1300** (0.005%). Since **SiRos1300** and **SiRosVDMA** have similar absorption and emission energies, the difference in Φ values can be compared without Energy Gap Law concerns being considered.[14] Effects such as vibrational energies of C–H bonds causing excited state relaxation of the dye can provide a pathway for non-radiative relaxation and many of the highest energy C–H vibrations are observed to be on the nitrogen containing donor groups.[15] It is not apparent if the C–H vibrations associated with indolizine are more strongly coupled to the excited state than with VDMA. Also, the steric interactions near the donor-core bond are reduced for VDMA and a more planarized conformation can be accessed which may also help with increasing quantum yields. Due to the

Table 2. Photophysical properties of SiRos dyes and literature benchmarks in CH_2Cl_2.

Dye	λ_{abs} (nm)	λ_{em} (nm)	ε ($M^{-1}cm^{-1}$)	Φ (%)	MB ($M^{-1}cm^{-1}$)	Stokes shift (eV | nm)
SiRosDMA	1002	1125	128500	0.030	38.6	0.14 | 123
SiRosVDMA	1154	1312	141000	0.029	40.9	0.13 | 158
SiRos1300[7]	1140	1300	115000	0.005	6.4	0.14 | 160
VIX-3[3e]	870	1070	177000	0.110	195	0.27 | 200
RhIndz ethyl ester[9c]	921	1086	97500	0.030	29.3	0.20 | 165
SiRos1700[7]	1440	1700	98000	0.001	1.1	0.13 | 260

higher quantum yields and molar absorptivities of **SiRosDMA** and **SiRosVDMA**, higher MB values are observed at 38.6 $M^{-1}cm^{-1}$ and 40.9 $M^{-1}cm^{-1}$, respectively, as compare to benchmark dye **SiRos1300** (6.4 $M^{-1}cm^{-1}$). Higher MB values are desirable for increasing the signal strength during optical imaging.

To demonstrate the suitability of this dye design for *in-vivo* biological imaging, nanoencapsulation of **SiRosDMA** is shown as an example allowing for absorption and emission in water (Figure S12). Notably, photophysical properties can differ significantly between organic and aqueous media.[16] Encapsulation of the dye in water-soluble nanoparticles was done by using Triton X100 as a polymer encapsulating agent to form dye-Triton X100 micelles.[5,17] Nanoencapsulated **SiRosDMA** with Triton X100 has an absorption maximum at 1052 nm in water, which is 50 nm longer wavelength than the absorption maximum of **SiRosDMA** in DCM. Both absorption and emission profiles in water and DCM have similar features and shapes. The emission maximum for **SiRosDMA** in DCM (1125 nm) and **SiRosDMA**-Triton X100 micelles in water (1120 nm) is similar at just 5 nm difference. The closer absorption and emission maximum of nanoencapsulated **SiRosDMA** indicates a smaller Stokes shift due to less reorganization upon photoexcitation presumably due to the confined space of the micelle.

The electrochemical properties of the SiRos dyes were analyzed via cyclic voltammetry in dichloromethane to analyze the effect of the donor groups on the frontier orbitals of the SiRos dyes (Table 3, Figure 4). All dyes demonstrate reversible reduction and oxidation waves during cyclic voltammetry. The ground state oxidation potential ($E_{(S+/S)}$) values were observed to be closely grouped within 50 mV from −0.47 V to −0.42 V versus ferrocenium/ferrocene with the following trend **SiRosDMA** < **SiRos1300** < **SiRosVDMA**. More electron rich (or less stabilized HOMO) dyes are anticipated to shift the $E_{(S+/S)}$ values toward more negative numbers versus ferrocene indicating the order of ease of oxidation is as follows: **SiRosDMA** < **SiRos1300** < **SiRosVDMA**. Notably, the values are close in potential, but tracks with the absorption maxima values . However, **SiRosDMA** being more easily oxidized than **SiRosVDMA** suggest that sterics may play a significant role in determining the oxidation potential and that the electron deficient core is better coupled to the more planar VDMA which makes the donor harder to oxidize. The ground state reduction potential ($E_{(S/S-)}$) values were observed at −1.61 V, −1.68 V and −1.76 V for **SiRosVDMA**, **SiRos1300** and **SiRosDMA** dye, respectively. The difference in reduction potential at 150 mV is greater than the difference in oxidation potential values of 50 mV. Since the core remains the same, the difference in $E_{(S/S-)}$ values is attributed to changes in conjugation length where the more conjugated donors (VDMA and indolizine) have more positive $E_{(S/S-)}$ values.

Table 3. Electrochemical properties of the SiRos dyes.

Dye	$E_{(S+/S)}$ (V vs $Fc^{+/0}$)	$E_{(S/S-)}$ (V vs $Fc^{+/0}$)
SiRosDMA	−0.47	−1.76
SiRosVDMA	−0.42	−1.61
SiRos1300	−0.45	−1.68

The effect of changing core atoms (oxygen versus silicon) and changing donors is compared via literature to enable a better understand of dye design approaches and the resulting photophysical properties. **SiRosVDMA** and **VIX-3** both have VDMA donors but differ at the core with **VIX-3** having an oxygen-based xanthene core (Figure 1). Notably, the aryl group appended to the xanthene or Si-substituted xanthene core changes; however, this group is out of the larger π-conjugated plane and has minimal effect on the dye absorption properties. Changing from the xanthene core to the Si-substituted xanthene core results in a 284 nm (0.50 eV) shift in the absorption maxima to longer wavelengths (Table 2). Similar shifts to longer wavelengths for the absorption and emission maxima is observed for **RhIndz Ethyl Ester** and **SiRos1300** where both dyes have indolizine donors and differ by the substitution of oxygen for silicon at the core (Table 2).[9c] The shift in absorption (and emission) upon exchanging oxygen and silicon correlates with prior literature reports.[8] Exchanging VDMA for indolizine donors (**SiRosVDMA** versus **SiRos1300** and **VIX-3** versus **RhIndz ethyl ester**) results in only modest changes of < 0.04 eV. Changing from DMA to VDMA or indolizine results in lower energy excitations by ~0.25 eV. The Φ values observed are about 4–6 times larger for DMA based donors relative to indolizine based donors. Similarly, the MB values are 6–7 times larger for the DMA donors. However, the indolizine donor groups are much more tunable with added conjugated substituents on the periphery allowing access to substantially longer emission wavelengths (~1700 nm).[7] Such a peripheral

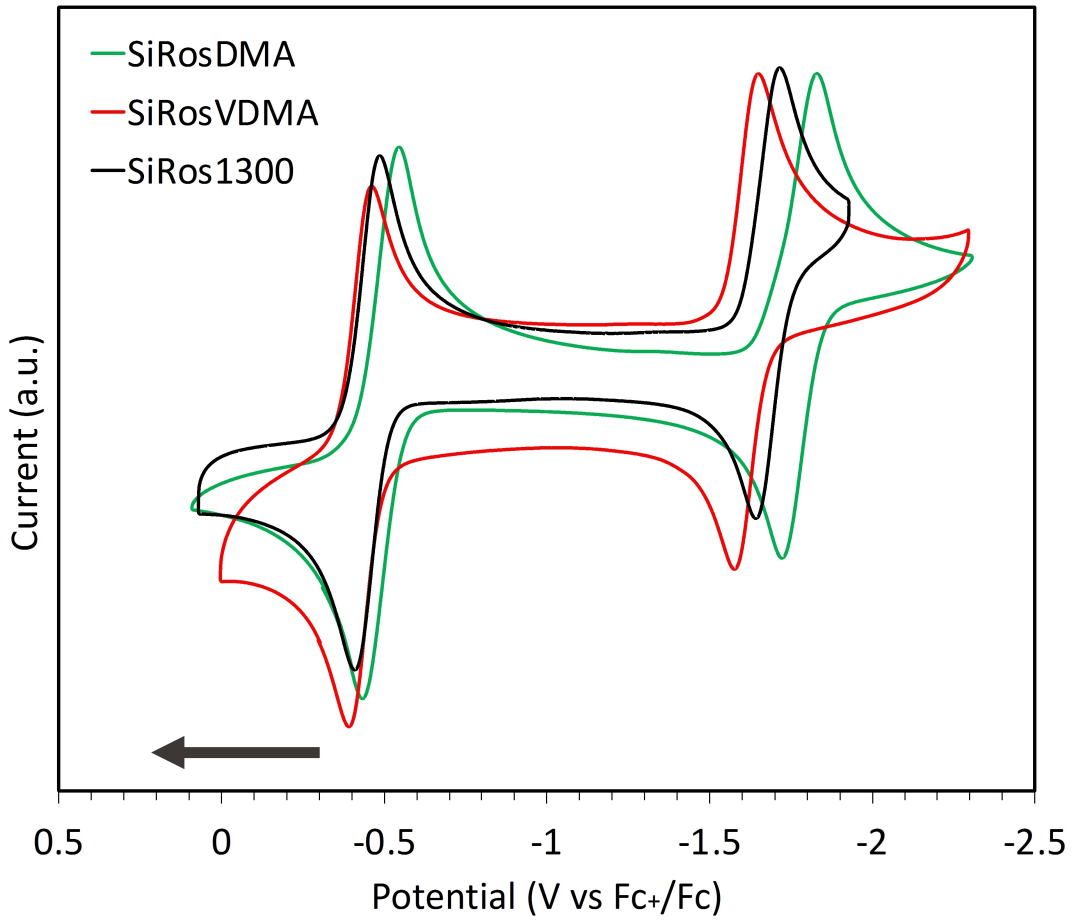

Figure 4. Cyclic voltammograms for **SiRosDMA**, **SiRosVDMA** and **SiRos1300** dyes in DCM. The arrow on the graph indicates the initial scanning direction with the arrow tail being the starting point of the scan.

extended conjugation strategy is not amenable to DMA type donors. Thus, if an application needs longer wavelength access, then indolizine donors are well-suited for use in dye designs. However, if higher MBs and Φs are needed and inherently shorter wavelength access can be allowed by the application, then VDMA type donors would be more suitable. This study has focused on a donor design for extending conjugation on the periphery of the donor to access longer wavelengths. However, we note that non-peripheral conjugation extended donor analogues to DMA, such as julolidine, can allow access to longer wavelengths too as demonstrated with a comparison of **VIX-3** (DMA-based) and **VIX-4** (julolidine-based) emission wavelengths (1070 nm versus 1210 nm, respectively).[3e]

Conclusions

Two novel Si-substituted xanthene-based SWIR dyes based on DMA and VDMA donors were synthesized and characterized photophysically, electrochemically, and computationally and compared with the literature dye **SiRos1300** with an indolizine donor to study the effect of donor choice on dye properties. The extended conjugation of the VDMA group relative to the DMA group resulted in a 0.16 eV bathochromic shift in the absorption and emission spectra maxima (absorbance maxima shifts from 1002 nm to 1154 nm). Incorporation of the indolizine donor, which has the same number of π-bonds on the donor as VDMA, gave a dye with absorption and emission maxima very close in energy to **SiRosVDMA**. The quantum yield of **SiRosVDMA** is significantly higher than that of **SiRos1300** and is attributed to the increased planarity of the **SiRosVDMA** dye. Notably, the indolizine donor is readily further functionalized to give derivatives of **SiRos1300** emitting at 1700 nm, but such modifications to DMA donors to induced shifts of absorption and emission to longer wavelengths are not obviously employable. In summary, VDMA provides a shift to longer wavelength access without a loss of quantum yield compared to DMA, but has limited tunability. The indolizine donor provides a more tunable system that can reach significantly longer wavelengths than VDMA, but has a reduced quantum yield. As already noted in the literature, the Si-substituted xanthene-based dyes gave much lower energy absorbing and emitting dyes than the oxygen-based xanthene core dyes found in the literature (a $>$200 nm shift to longer wavelength for the current examples). Finally, the nanoencapsulation of **SiRosDMA** in Triton X100 allowed for the measurement of absorption and emission properties in water as necessary for *in-vivo* biological imaging. Future work will focus on modification of the indolizine donor

to give a vinyl-indolizine structure which would both reduce the steric strain between the xanthene core and indolizine donor to give a higher quantum yield dye and also allow access to longer wavelengths. Additionally, removing the out-of-plane phenyl ring from indolizine that is present as a stabilizing feature to some of the synthetic intermediates could also raise quantum yield. Both approaches will likely require restructured synthetic routes based on attempts in our labs. Ideally, the phenyl group could be removed, the vinyl group installed, and donors added to the 1 and 7 positions of the indolizine to allow for deep SWIR access.

Experimental Section

General Experimental Information. All commercially obtained reagents and solvents were used as received without further purification. Si-xanthene core (**1**) was synthesized according to the literature procedure with ^{1}H NMR data collected in agreement with the reported values.[7] Compound **2** and **4** are commercially available and were purchased from Sigma Aldrich. Thin-layer silica gel chromatography (TLC) was conducted with Sorbent Technologies, Inc. (Atlanta, GA, USA) glass-backed 250 μm Silica Gel XHL TLC plates and utilized a UV (254 nm) indicator to visualize. ^{1}H, ^{31}P, ^{19}F, and ^{13}C NMR spectra were recorded on a Bruker Avance-300 (300 MHz) spectrometer and a Bruker Avance-400 (400 MHz) spectrometer and are reported in ppm using solvent as an internal standard (chloroform-*d*, $CDCl_3$ at 7.26 ppm; DCM-d_2 CD_2Cl_2 at 5.29 ppm and acetonitrile-d_3, CD_3CN at 1.94 ppm for ^{1}H NMR) and (chloroform-*d*, $CDCl_3$ δ = 77.16 ppm, acetonitrile-d_3, CD_3CN at 1.57 ppm for ^{13}C NMR). Data are reported as s = singlet, d = doublet, t = triplet, sept = septet, m = multiplet, and br = broad; coupling constants (J) are in Hz; and integration. Flash column chromatography was performed on a Teledyne Combi Flash Rf+ with prepacked Silica Luknova SuperSep 12–80 g cartridges. Short plugs of silica were performed with Sorbtech technical grade 60 Å pore size (230×400 mesh) silica gel. For electrospray ionization (ESI) high-resolution mass spectrometry (HRMS), quadruple-TOF was used to obtain the data both in positive and negative modes with a Waters Synapt HDMS. The mass analyzer was set to the 200–2000 Da range. Infrared spectra were recorded with a Bruker α Platinum-ATR FTIR spectrometer and spectra processed on OPUS 6.5 software. UV–Vis–NIR spectra were measured with a Cary 5000 UV–vis–NIR spectrometer. All molar absorptivity measurements were calculated using the Beer–Lambert law equation at three different concentrations plotted with a linear fit ($R^2 > 0.99$) whose slope gave the molar absorptivity of the respective dye and the values reported are rounded to the nearest 500 $M^{-1}cm^{-1}$. The emission data for **SiRosDMA** and **SiRosVDMA** was collected using a Horiba PTI QuantaMaster QM-8075-21 fluorometer with a liquid nitrogen cooled InGaAs detector that used a 992 nm excitation source, an excitation slit width of 10 mm, and an emission slit width of 15 mm, with IR-1061 in CH_2Cl_2 as the reference dye (Φ = 0.32 %).[13] Rectangular 10 mm path cuvettes were used for all fluorescence measurements. The photoluminescent quantum yields (PLQY) of the dyes were calculated using the integrated emission intensity values (summation of all Y-value data points using Microsoft Excel) by using the following relative quantum yield equation:[18]

$$\Phi_{sample} = \Phi_{reference} \times \frac{E_{sample}}{E_{reference}} \times \frac{S_{reference}}{S_{sample}} \times \frac{\eta^2_{sample}}{\eta^2_{reference}}$$

where Φ_F denotes the quantum yield; *E* refers to integrated emission intensity; *S* is equal to $1–10^{-A}$, with the superscript A being the absorbance value at the excitation wavelength; η is the refractive index of the solvent; sample is the dye studied herein; and reference is the reference standard (IR1061) chosen for quantum yield studies. The absorbances were 0.10–0.42 at the excitation wavelength for both the dye emission samples. Optical data for **SiRos1300** has been previously reported in the literature with data available at https://zenodo.org/records/10079855.[7] The absorption and emission data were collected under air.

General Computational Information. Molecules were drawn in ChemDraw (20.1) and saved as an MDL Molfile. These geometries were then optimized with the MMFF94 force field via Avogadro (1.2.0). Dihedral angles about noncyclic single bonds were set to between 0 and 90 degrees manually to avoid local minima conformations. Accurate geometry optimization was performed sequentially by DFT using Guassian 16 software[11] with the B3LYP functional[10a,b] with the following basis sets: first 3-21g, second 6-31g (d,p)[10c,19] and finally 6-311g (d,p)[20] all in dichloromethane as a polarizable continuum model (PCM).[21] TD-DFT computations were performed with optimized geometries with the B3LYP functional and 6-311g (d,p) basis set to compute vertical transition energies and oscillator strengths. Frequency calculations reveal no imaginary frequencies.

*Nanoencapsulated **SiRosDMA** Protocol.* 1 mM of **SiRosDMA** in chloroform and 3 mM of Triton X100 in chloroform were mixed in a ratio of 1 : 40 (**SiRosDMA**:Triton X100). The chloroform was evaporated from the mixture by nitrogen flow into the mixture. After evaporation of chloroform from the mixture, the paste was dissolved in water then absorption and emission spectrum of the encapsuled dye were obtained.[5,17]

Electrochemical data information. Cyclic voltammetry curves were measured with a C–H Instruments electrochemical analyzer Model CHI602E. Tetrabutylammonium hexafluorophosphate (0.1 M in dichloromethane) was used as the electrolyte. The working electrode is glassy carbon, the pseudo-reference electrode is a silver wire, and the counter electrode is platinum. All measurements were conducted under an argon atmosphere with a scan rate of 100 mV/s and cyclic voltammograms were initiated from approximately −0.30 V versus Fc^+/Fc and were scanned initially in the positive direction. Ferrocenium/ferrocene is used as a reference standard and taken as 0.00 V and oxidation and reduction potentials of the materials are reported versus Fc^+/Fc^0 in DCM.

Synthetic Procedures. 3,7-bis(4-(dimethylamino)phenyl)-5,5-bis(2-ethylhexyl) dibenzo[*b*,*e*]silin-10(5*H*)-one (**3**): To a pressure flask under N_2, with a stir bar, Na_2CO_3 (0.318 g, 3.0 mmol) was added in H_2O (1.8 mL) while purging under N_2 for 5 minutes. Then, Si-substituted xanthene core **1** (0.300 g, 0.6 mmol) and *N*, *N*-dimethyl-4-(4,4,5,5 tetramethyl-1,3,2-dioxaborolan-2-yl) aniline **2** (0.311 g, 1.26 mmol) were added with a toluene:ethanol (1 : 1, 18 mL) solvent mixture. $Pd(dba)_2$ (0.017 g, 0.03 mmol) and X-Phos (0.028 g, 0.06 mL) were then added under N_2. The pressure flask reaction mixture was degassed with N_2 for 5 minutes before sealing the pressure flask. The reaction was allowed to stir at 100 °C and was monitored by NMR until all of the starting material was observed to be consumed. After 12 hours, the reaction was cooled to room temperature and water was added and the reaction mixture was extracted with CH_2Cl_2 thrice. The CH_2Cl_2 layer was dried with sodium sulfate and concentrated to yield the crude product. The crude product was purified by using silica gel chromatography with 50 % DCM/50 % hexanes to obtain a yellow product (0.287 g, 0.43 mmol) in 71 % yield. ^{1}H NMR (400 MHz, $CDCl_3$, Figure S1) δ 8.54 (d, *J* = 8.4 Hz, 2H), 7.85 (s, 2H), 7.78 (d, *J* = 8.4 Hz, 2H), 7.63 (d, *J* = 8.7 Hz, 4H), 6.86 (d, *J* = 8.7 Hz, 4H), 3.04 (s, 12 H), 1.35–1.26 (m, 2H), 1.16–0.92 (m, 20H),

0.65–0.62 (m, 12H) ppm. ^{13}C NMR (101 MHz, $CDCl_3$, Figure S2) δ 187.2, 150.5, 143.5, 139.2, 139.1, 138.9, 138.8, 130.9, 128.0, 127.9, 127.5, 112.7, 40.5, 35.3, 35.2, 28.8, 28.5, 28.4, 22.8, 19.2, 14.0, 10.6 ppm. Note that there are multiple diastereomers present due to the stereocenters on the alkyl chains. These stereocenters do not significantly affect the photophysical properties measured herein as they are part of the non-conjugated system, but they do result in additional ^{13}C NMR peaks being observed for a few carbon signals. HRMS m/z $[M+H]^+$ Calcd., C45H61N2OSi 673.4553; found, 673.4559. IR (neat, cm^{-1}) 3047, 2956, 2924, 2856, 2806, 1682, 1634, 1609, 1583, 1523, 1481, 1458, 1444, 1356, 1284, 1264, 1226, 1197, 1168, 1142, 1074, 1062, 947, 926, 862, 786, 734, 687, 588, 526.

N-(4-(7-(4-(dimethylamino)phenyl)-10-(2,6-dimethylphenyl)-5,5-bis(2-ethylhexyl)dibenzo [*b*,*e*]silin-3(5*H*)-ylidene)cyclohexa-2,5-dien-1-ylidene)-*N*-methylmethanaminium hexafluorophosphate (**SiRosDMA**): To a flame dried pressure flask, was added compound **3** (98 mg, 0.146 mmol, 1 equiv.) and THF (0.04 M, 3.7 mL). The solution was degassed with N_2 for 5 minutes, and then 10 equiv. of 2,6-dimethylphenylmagnesium bromide (1.46 mL, 1.0 M in THF) was added to the mixture dropwise with constant stirring under N_2. The reaction was stirred and heated at 100 °C and monitored via NMR until completion. After 10 hours, reaction was quenched with water, and the reaction mixture was diluted using DCM. The DCM layer was extracted, and the organic layer was dried over Na_2SO_4 and concentrated under reduced vacuum. To the crude product was added dry dichloroethane (3.7 mL, 0.02 M) in a pressure flask, and then $POCl_3$ was added (0.02 mL, 0.22 mmol) dropwise. The solution was degassed with N_2 for 10 min and then heated at 60 °C for 2 hours under a N_2 atmosphere. The volatiles were evaporated via a rotary evaporator. Then, the reaction mixture was dissolved in dry dichloromethane. Excess potassium hexafluorophosphate dissolved in minimum acetonitrile was added into the reaction mixture with stirring at room temperature for one hour. Any salts were filtered and the volatiles were removed under reduced pressure. The crude product was purified via flash silica gel column chromatography with 5% acetonitrile/95%dichloromethane as the eluent to give the desired dye as a green solid. Further, purification was performed by dissolving the concentrated product in a minimal amount of dichloromethane followed by the addition of excess of diethyl ether at 0 °C and allowing the solution rest for half an hour. The pure product is insoluble in ether and slowly precipitates from the solution and is isolated by vacuum filtration. (63%, 0.121 g, 0.092 mmol). ^{1}H NMR (400 MHz, CD_3CN, Figure S3) δ 8.41 (ap dt, J= 6.3, 2.3 Hz, 2H), 8.05 (d, J=9.4 Hz, 4H), 7.79 (d, J=9.1 Hz, 2H), 7.47 (t, J=7.6 Hz, 1H), 7.32 (t, J=8.6 Hz, 4H), 6.97 (d, J=9.4 Hz, 4 H), 3.21 (s, 12 H), 2.01 (s, 6H), 1.43–1.33 (m, 6H), 1.15–1.03 (m, 12 H), 0.90–0.78 (m, 4H), 0.66 (t, J=6.9 Hz, 6H), 0.60 (t, J=7.2 Hz, 6H) ppm. ^{13}C NMR (101 MHz, CD_3CN, Figure S4) δ 153.5, 148.6, 148.4, 148.2, 139.8, 139.9, 137.6, 136.3, 133.9, 131.5, 129.7, 128.2, 127.3, 124.6, 114.2, 40.4, 36.1, 35.5, 35.6, 29.3, 28.3, 23.1, 19.7, 19.5, 13.9, 10.9 ppm. One of the aromatic ^{13}C signals is likely under the MeCN signal near 117 ppm and could be presenting as a slight shoulder. ^{19}F NMR (376 MHz, CD_3CN, Figure S5) shifts were δ–72.73 for (d, J=833 Hz, 6F). ^{31}P NMR (162 MHz, CD_3CN, Figure S6) shifts were δ −144.61 (sept, J=707 Hz, 1P). HRMS (ESI) m/z: $[M]^+$ Calcd., C53H69N2Si 761.5225; found, 761.5223. IR (neat, cm^{-1}) 3418, 3219, 3083, 2955, 2924, 2859, 2811, 2668, 2638, 2585, 2549, 2529, 2483, 2210, 2129, 2025, 1887, 1811, 1729, 1605, 1578, 1526, 1461, 1441, 1351, 1328, 1281, 1237, 1216, 1184, 1089, 1063, 943.

3,7-bis((*E*)-4-(dimethylamino)styryl)-5,5-bis(2-ethylhexyl)dibenzo[*b*,*e*]silin-10(5*H*)-one (**5**): In a flame dried pressure flask under N_2, Si-substituted xanthone core **1** (1.9 g, 3.8 mmol) was added with *N*, *N*-dimethyl-4-vinylaniline, **4** (1.52 g, 7.98 mmol), Pd(t-$Bu_3P)_2$ (0.39 g, 0.76 mmol), and Cy_2NMe (1.8 mL, 8.36 mmol) in dioxane (2.7 mL, 1.4 M). The reaction was stirred for 12 hours at 120 °C. After all the starting material was consumed, the reaction mixture was extracted with DCM and H_2O. The DCM layer was concentrated under reduced pressure to give the crude product. The crude product was purified by using flash silica gel column chromatography at 50% DCM/50% hexanes to obtain the pure yellow fluorescent product (2.5 g, 3.4 mmol, 89% yield). ^{1}H NMR (300 MHz, $CDCl_3$, Figure S7) δ 8.46 (d, J=9.1 Hz, 2H), 7.71–7.67 (m, 4H), 7.48 (d, J=8.9 Hz, 4H), 7.22 (d, J=16.2 Hz, 2H), 6.99 (d, J= 16.2 Hz, 2H), 6.74 (d, J=11.9 Hz, 4H), 3.01 (s, 12H), 1.34–1.23 (m, 2H), 1.12–1.01 (m, 20 H), 0.71-0.63 (m, 12H) ppm. ^{13}C NMR (76 MHz, CDCl3, Figure S8) δ 186.7,150.5, 140.8, 139.7, 138.9, 138.8, 131.5, 130.3, 128.0, 126.8, 125.2, 123.3, 112.3, 40.4, 35.2, 32.2, 28.8, 28.4, 22.8, 19.2, 14.1, 10.6 ppm HRMS (ESI) m/z: $[M + H]^+$ Calcd., C49H65N2OSi 725.4866; found, 725.4865. IR (neat, cm^{-1}) 3249, 3205, 3182, 3152, 3075, 3027, 2953, 2921, 2854, 2804, 2644, 1632, 1605, 1575, 1520, 1479, 1457, 1388, 1356, 1238, 1218, 1064, 947, 928.

N-(4-((*E*)-2-(7-((*E*)-4-(dimethylamino)styryl)-10-(2,6-dimethylphenyl)-5,5-bis(2-ethylhexyl)dibenzo[*b*,*e*]silin-3(5*H*)-ylidene)ethylidene)cyclohexa-2,5-dien-1-ylidene)-*N*-methylmethanaminium hexafluorophosphate (**SiRosVDMA**): To a flame dried pressure flask, was added Si-substituted xanthone **5** (0.200 g, 0.25 mmol, 1 equiv.) and THF (0.04 M, 6.1 mL). The solution was degassed with N_2 for 5 minutes, and then 2,6-dimethylphenylmagnesium bromide (3.68 mL, 1.0 M in THF) was added to the mixture dropwise with constant stirring under N_2. The reaction was stirred at 100 °C and monitored via NMR until completion. After 10 hours, the reaction was quenched with water, and the reaction mixture was diluted using DCM. The DCM layer was extracted from water, passed through a short silica plug, dried over Na_2SO_4 and then concentrated under reduced vacuum. To the crude material was added dry dichloroethane (5.25 mL, 0.02 M) in a pressure flask under N_2, and $POCl_3$ was added (0.03 mL, 0.32 mmol) slowly dropwise. The solution was degassed with N_2 for 10 min and then heated at 60 °C for 2 hours under a N_2 atmosphere. After cooling the reaction mixture to room temperature, the reaction mixture was dissolved in dry dichloromethane. Then, excess potassium hexafluorophosphate dissolved in minimum acetonitrile was added to the reaction mixture. The mixture was stirred at room temperature for one hour. Any salts were filtered, and the volatiles were removed under reduced pressure. The crude product was purified via flash silica gel column chromatography with 5% acetonitrile/95% dichloromethane as the eluent to give the desired dye as a dark pink solid in 49% yield (0.100 g, 0.123 mmol). The dye could be dissolved in minimal DCM and precipitation from diethyl ether to raise purity if needed. ^{1}H NMR (400 MHz, CD_2Cl_2, Figure S9) δ 7.87 (s, 2H), 7.68 (d, J=15.2 Hz, 2H), 7.61 (d, J=9.2 Hz, 4H), 7.41 (t, J= 8.1 Hz, 1H), 7.38 (d, J=7.4 Hz, 2H), 7.25–7.20 (m, 4H), 7.09 (d, J= 15.8 Hz, 2H), 6.78 (d, J=9.2 Hz, 4H), 1.91 (s, 6H), 1.51 (s, 8H), 1.37–1.36 (2H), 1.26–0.89 (m, 22H), 0.70–0.64 (m, 12H) ppm. ^{13}C NMR was not obtained due to poor resolution at the high concentration needed for a ^{13}C NMR spectrum on a reasonable time scale presumably due to dye aggregation. ^{19}F NMR (376 MHz, CD_2Cl_2, Figure S10) δ (−73.43) (d, J=709.2 Hz, 6F). ^{31}P NMR (162 MHz, CD_2Cl_2, Figure S11) δ (−144.47) (sept, J=710.2 Hz, 1P). HRMS (ESI) m/z: $[M]^+$ Calcd., $C_{57}H_{73}N_2Si^+$ 813.5538; found, 813.5519. IR (neat, cm^{-1}) 3212, 3079, 3043, 2954, 2922, 2854, 2810, 2679, 1609, 1520, 1389, 1353, 1320, 1263, 1166, 1067, 1042, 969, 940, 908.

Supporting Information

The Supporting Information is available free of charge.

Acknowledgements

This research was supported by the CEMOs under the National Science Foundation (NSF) OIA EPS Track 1 grant number 1757220.

Conflict of Interests

Jared Delcamp has a patent (US20220370641) on the benchmarking dyes used in the manuscript.

Data Availability Statement

The data that support the findings of this study are available from the corresponding author upon reasonable request.

Keywords: dimethylaniline (DMA) · Si-substituted xanthene · NIR-II · SWIR · emission · quantum yield

[1] a) M. L. Yap, J. D. McFadyen, X. Wang, M. Ziegler, Y.-C. Chen, A. Willcox, C. J. Nowell, A. M. Scott, E. K. Sloan, P. M. Hogarth, *Theranostics* **2019**, *9*, 1154; b) D. A. Mankoff, *J. Nucl. Med.* **2007**, *48*, 18 N; c) K. Chen, X. Chen, *Curr. Top. Med. Chem.* **2010**, *10*, 1227–1236.
[2] a) A. L. Antaris, H. Chen, K. Cheng, Y. Sun, G. Hong, C. Qu, S. Diao, Z. Deng, X. Hu, B. Zhang, *Nat. Mater.* **2016**, *15*, 235–242; b) J. Gayton, S. A. Autry, W. Meador, S. R. Parkin, G. A. Hill Jr, N. I. Hammer, J. H. Delcamp, *J. Org. Chem.* **2018**, *84*, 687–697; c) A. B. Braun, I. Wehl, D. K. Kölmel, U. Schepers, S. Bräse, *Chem. Eur. J.* **2019**, *25*, 7998–8002; d) R. Alford, H. M. Simpson, J. Duberman, G. C. Hill, M. Ogawa, C. Regino, H. Kobayashi, P. L. Choyke, *Mol. Imaging* **2009**, *8*, doi: 10.2310/7290.2009.00031; e) X. Tian, L. C. Murfin, L. Wu, S. E. Lewis, T. D. James, *Chem. Sci.* **2021**, *12*, 3406–3426; f) L. Wang, M. S. Frei, A. Salim, K. Johnsson, *J. Am. Chem. Soc.* **2018**, *141*, 2770–2781; g) Y. Yang, F. Gao, Y. Wang, H. Li, J. Zhang, Z. Sun, Y. Jiang, *Molecules* **2022**, *27*, 8421.
[3] a) J. Zhao, D. Zhong, S. Zhou, *J. Mater. Chem. B* **2018**, *6*, 349–365; b) S. Zhu, R. Tian, A. L. Antaris, X. Chen, H. Dai, *Adv. Mater.* **2019**, *31*, 1900321; c) H. Dai, Q. Shen, J. Shao, W. Wang, F. Gao, X. Dong, *Innovation* **2021**, *2*, 100179; d) M. J. Schnermann, *Nature* **2017**, *551*, 176–177; e) D. Liu, Z. He, Y. Zhao, Y. Yang, W. Shi, X. Li, H. Ma, *J. Am. Chem. Soc.* **2021**, *143*, 17136–17143.
[4] a) T. Terai, T. Nagano, *Curr. Opin. Chem. Biol.* **2008**, *12*, 515–521; b) J. Chan, S. C. Dodani, C. J. Chang, *Nat. Chem.* **2012**, *4*, 973–984.
[5] S. Chatterjee, A. K. Shaik, K. H. Wijesinghe, D. Ndaleh, A. Dass, N. I. Hammer, J. H. Delcamp, *J. Org. Chem.* **2022**, *87*, 11319–11328.
[6] a) C. Sun, B. Li, M. Zhao, S. Wang, Z. Lei, L. Lu, H. Zhang, L. Feng, C. Dou, D. Yin, *J. Am. Chem. Soc.* **2019**, *141*, 19221–19225; b) J. A. Carr, M. Aellen, D. Franke, P. T. So, O. T. Bruns, M. G. Bawendi, *Proc. Nat. Acad. Sci.* **2018**, *115*, 9080–9085.
[7] W. E. Meador, E. Y. Lin, I. Lim, H. C. Friedman, D. Ndaleh, A. K. Shaik, N. I. Hammer, B. Yang, J. R. Caram, E. M. Sletten, J. H. Delcamp, *Nat. Chem.* **2024**, DOI: 10.1038/s41557-41024-01464-41556.
[8] M. Fu, Y. Xiao, X. Qian, D. Zhao, Y. Xu, *Chem. Commun.* **2008**, 1780–1782.
[9] a) M. A. Saucier, C. Smith, N. A. Kruse, N. I. Hammer, J. H. Delcamp, *Molecules* **2023**, *28*, 1287; b) D. Ndaleh, C. Smith, M. Loku Yaddehige, A. K. Shaik, D. L. Watkins, N. I. Hammer, J. H. Delcamp, *J. Org. Chem.* **2021**, *86*, 15376–15386; c) C. S. Rathnamalala, J. N. Gayton, A. L. Dorris, S. A. Autry, W. Meador, N. I. Hammer, J. H. Delcamp, C. N. Scott, *J. Org. Chem.* **2019**, *84*, 13186–13193.
[10] a) A. Becke, *J. Chem. Phys.* **1993**, *98*, 5648–5652; b) C. Lee, W. Yang, R. G. Parr, *Phys. Rev. B* **1988**, *37*, 785; c) W. J. Hehre, R. Ditchfield, J. A. Pople, *J. Chem. Phys.* **1972**, *56*, 2257–2261.
[11] M. J. T. Frisch, G. W. Trucks, H. B. Schlegel, G. E. Scuseria, M. A. Robb, J. R. Cheeseman, G. Scalmani, V. Barone, G. A. Petersson, H. Nakatsuji, X. Li, M. Caricato, A. V. Marenich, J. Bloino, B. G. Janesko, R. Gomperts, B. Mennucci, H. P. Hratchian, J. V. Ortiz, A. F. Izmaylov, J. L. Sonnenberg, D. Williams-Young, F. Ding, F. Lipparini, F. Egidi, J. Goings, B. Peng, A. Petrone, T. Henderson, D. Ranasinghe, V. G. Zakrzewski, J. Gao, N. Rega, G. Zheng, W. Liang, M. Hada, M. Ehara, K. Toyota, R. Fukuda, J. Hasegawa, M. Ishida, T. Nakajima, Y. Honda, O. Kitao, H. Nakai, T. Vreven, K. Throssell, J. A. Montgomery, Jr., J. E. Peralta, F. Ogliaro, M. J. Bearpark, J. J. Heyd, E. N. Brothers, K. N. Kudin, V. N. Staroverov, T. A. Keith, R. Kobayashi, J. Normand, K. Raghavachari, A. P. Rendell, J. C. Burant, S. S. Iyengar, J. Tomasi, M. Cossi, J. M. Millam, M. Klene, C. Adamo, R. Cammi, J. W. Ochterski, R. L. Martin, K. Morokuma, O. Farkas, J. B. Foresman, D. J. Fox, Gaussian 16, revision: A.03; Gaussian, Inc.: Wallingford CT, 2016.
[12] M. Ventura, J. Silva, T. Catunda, L. Andrade, S. Lima, *J. Mol. Liq.* **2021**, *328*, 115414.
[13] E. D. Cosco, J. R. Caram, O. T. Bruns, D. Franke, R. A. Day, E. P. Farr, M. G. Bawendi, E. M. Sletten, *Angew. Chem. Int. Ed.* **2017**, *56*, 13126–13129.
[14] a) C. Erker, T. Basché, *J. Am. Chem. Soc.* **2022**, *144*, 14053–14056; b) E. Thimsen, B. Sadtler, M. Y. Berezin, *Nat. Photonics* **2017**, *6*, 1043–1054; c) J. R. Lakowicz, *Principles of fluorescence spectroscopy*, Springer, **2006**.
[15] H. C. Friedman, E. D. Cosco, T. L. Atallah, S. Jia, E. M. Sletten, J. R. Caram, *Chem* **2021**, *7*, 3359–3376.
[16] M. V. Bobo, A. M. Arcidiacono, P. J. Ayare, J. C. Reed, M. R. Helton, T. Ngo, K. Hanson, A. K. Vannucci, *ChemPhotoChem* **2021**, *5*, 51–57.
[17] S. Ansteatt, A. Meares, M. Ptaszek, *J. Org. Chem.* **2021**, *86*, 8755–8765.
[18] C. A. Parker, W. Rees, *Analyst* **1960**, *85*, 587–600.
[19] M. M. Francl, W. J. Pietro, W. J. Hehre, J. S. Binkley, M. S. Gordon, D. J. DeFrees, J. A. Pople, *J. Chem. Phys.* **1982**, *77*, 3654–3665.
[20] M. J. Frisch, J. A. Pople, J. S. Binkley, *J. Chem. Phys.* **1984**, *80*, 3265–3269.
[21] a) S. Miertuš, E. Scrocco, J. Tomasi, *Chem. Phys.* **1981**, *55*, 117–129; b) S. Miertus, J. Tomasi, *Chem. Phys.* **1982**, *65*, 239–245; c) J.-L. Pascual-ahuir, E. Silla, I. Tunon, *J. Comput. Chem.* **1994**, *15*, 1127–1138.

Manuscript received: January 28, 2024
Revised manuscript received: March 16, 2024
Accepted manuscript online: March 26, 2024
Version of record online: June 7, 2024